The use of C_6D_6 detectors for neutron induced capture cross-section measurements in the resonance region

A. Borella[a,b], G. Aerts[b], F. Gunsing[b], M. Moxon[c], P. Schillebeeckx[a,*], R. Wynants[a]

[a]EC-JRC-IRMM, Retieseweg 111, B-2440 Geel, Belgium
[b]CEA/Saclay, DSM/DAPNIA/SPhN, F-91911 Gif-sur-Yvette, France
[c]Hyde Copse 3, Marcham, UK

Abstract

Hydrogen-free deuterated benzene C_6D_6 liquid scintillators are widely used for high resolution neutron capture cross-section measurements at time-of-flight facilities, using the total energy detection principle in combination with the Pulse Height Weighting Technique (PHWT). The quality of the data deduced from such measurements depends on the accuracy of the detector response that is used in the calculation of the weighting function and on the normalization procedure. In addition, for nuclei with small capture to scattering ratios, i.e. light and near neutron magic nuclei, a correction for the sensitivity of the capture detector to the scattered neutrons is required. The MCNP code was used to simulate both the γ-ray and neutron transport in a C_6D_6 detection system including its surroundings. The weighting functions and neutron sensitivity were then deduced from the simulations and validated by experiments. The simulations have also been used to identify the sources of uncertainties in performing capture cross-section measurements with C_6D_6 detectors.

1. Introduction

Neutron induced capture cross-section measurements rely either on post-irradiation activation analysis or on the detection of the prompt γ-rays emitted in the (n,γ) reaction. The study of the resonance structure of cross-sections requires high-resolution neutron energy dependent measurements. Experimentally, the resonance region is best studied at a pulsed white neutron source optimized for time-of-flight (TOF) measurements. An ideal capture detection system satisfies the following requirements [1,2]:

(1) The detection efficiency for a capture event should be independent of the subsequent γ-ray cascade, i.e. independent of the multiplicity of the γ-ray spectrum and the γ-ray energy distribution.
(2) The sensitivity to scattered neutrons should be as low as possible.
(3) The detector should have a very good timing response.

Three main groups of neutron capture detectors that have been used up to present are: high-resolution γ-ray detectors, total γ-ray absorption detectors and total energy detection systems.

Using high-resolution γ-ray Ge detectors, the capture cross-section can be determined for individual primary γ-rays depopulating the initial capturing state [3] or alternatively measuring all γ-rays feeding the ground state [4]. Recently Belgya proposed a new kind of intensity balance calculation, named crossing intensity sum [5]. Gamma-spectroscopic methods are only applicable to

*Corresponding author. Tel.: +32 14 571 475; fax: +32 14 571 862.
E-mail addresses: peter.schillebeeckx@ec.europa.eu,
peter.schillebeeckx@cec.eu.int (P. Schillebeeckx).

nuclei with a relatively simple and well known level scheme such that all the capture γ-rays are known and can be resolved. In addition, Ge detectors suffer from a relatively high sensitivity to neutrons.

Total absorption detectors rely on the detection of all γ-rays emitted in a capture event. The ideal detector has a 4π geometry and a 100% detection efficiency for all γ-rays in the cascade. Most of these detectors also have the ability to measure the multiplicity distribution of the γ-ray cascades. This feature was successfully exploited at the Kurchatov Institute by Muradyan et al. [6] using a multisectional detector based on 48 NaI(Tl) crystals. A similar system, containing 16 NaI(Tl) crystals, is used for capture cross-section measurements in the thermal and epi-thermal energy region at the TOF-facility of the Rensselaer Polytechnic Institute [7]. A detection assembly of 12 BGO-crystals is installed at the linear accelerator of the Kyoto University, Research Reactor Institute (KURRI) [8]. A BaF_2 detection system made of 42 individual crystals with a truncated pyramidal shape [9] is used at the FZK Karlsruhe to determine capture cross-sections in the unresolved resonance and high-energy region [10]. Capture measurements extended to applications in the resolved resonance region with a similar system have been performed at the n_TOF facility at CERN [11]. The Detector for Advanced Neutron Capture Experiments (DANCE), which is an 4π array consisting of 162 BaF_2 elements, has been installed at the Los Alamos Neutron Science Center (LANSCE) to carry out neutron capture cross-section measurements [12]. The initial design work of this detector and the one used at n_TOF is described in Ref. [13].

The total energy system is based on the use of low efficiency detectors with a γ-ray detection efficiency that is proportional to the γ-ray energy. The Moxon-Rae detector achieves approximately the proportionality between the γ-ray energy and detection efficiency by a proper design of the detector [14]. However, the use of this type of detectors has been abandoned due to the non-proportionality of the efficiency below 0.5 MeV and its low detection efficiency [2]. An alternative is the pulse height weighting technique by means of the so-called weighting function. This technique is based on an original suggestion by Maier–Leibnitz and was first applied by Macklin and Gibbons [15] using C_6F_6 detectors. Nowadays one prefers the use of the less neutron sensitive C_6D_6 detectors [2,16,17]. This paper discusses the total energy detection principle using C_6D_6 detection systems for the determination of neutron induced capture cross–sections in the resonance region based on experimental data obtained at the GELINA TOF-facility [18]. Such systems are also extensively used at ORELA [19], n_TOF at CERN [20] and at KURRI [21].

2. The total energy detection principle using C_6D_6 detectors

For a detection system with a low γ-ray detection efficiency ($\varepsilon_\gamma \ll 1$), such that at most only one γ-ray out of

the capture cascade is registered at a time, the efficiency to detect a capture event ε_c can be approximated by

$$\varepsilon_c = 1 - \prod_i (1 - \varepsilon_{\gamma i}) \approx \sum_i \varepsilon_{\gamma i}. \tag{1}$$

When in addition the efficiency to detect a γ-ray is directly proportional to the γ-ray energy E_γ

$$\varepsilon_\gamma = kE_\gamma \tag{2}$$

the detection efficiency for a neutron capture event becomes directly proportional to the sum of the energies of the γ-rays $E_{\gamma i}$ emitted in the capture event. Neglecting the internal conversion process, the detection efficiency becomes directly proportional to the total excitation energy E_x, which is the sum of the neutron binding energy S_n and the neutron energy $E_{n,c}$ in the center of mass system

$$\varepsilon_c \approx k \sum_i E_{\gamma i} \approx kE_x = k(S_n + E_{n,c}) \tag{3}$$

and independent of the actual cascade path.

As illustrated in Fig. 1, the γ-ray detection efficiency for a typical C_6D_6 detector is small, but not directly proportional with the γ-ray energy. However, this proportionality can be achieved through the pulse height weighting technique, i.e. the response function of the detection system is mathematically manipulated to achieve the proportionality between the detection efficiency and the γ-ray energy. A weighting function $W(E_d)$ is defined such that it follows the relationship:

$$\int_0^\infty R_d(E_d, E_\gamma)W(E_d)\mathrm{d}E_d = kE_\gamma \tag{4}$$

with $R_d(E_d, E_\gamma)$ the detector response, i.e. the probability that a γ-ray with an energy E_γ results in an observed deposited energy E_d. The proportionality factor k is usually taken equal to $1\,\mathrm{MeV}^{-1}$ when deriving $W(E_d)$. The overall efficiency $\varepsilon(E_\gamma)$ for detecting a γ-ray of energy E_γ
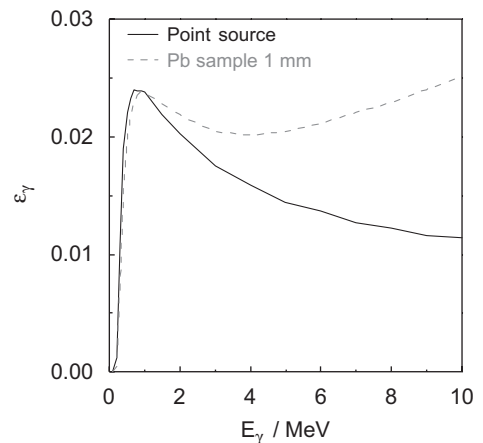

Fig. 1. The simulated γ-ray detection efficiency for a γ-ray emission from a point source and a homogeneous emission from a Pb disc (1 mm thick and 60 mm diameter). The detection system consists of 4 C_6D_6 detectors placed at $125°$ with respect to the direction of the incoming neutron beam.

corresponds to the integral of the function $R_d(E_d, E_\gamma)$

$$\int_0^\infty R_d(E_d, E_\gamma) dE_d = \varepsilon(E_\gamma). \tag{5}$$

In a neutron capture experiment at TOF-facilities the TOF is recorded together with the energy deposited in the detector. Using the weighting function defined in Eq. (4) a weighted TOF-spectrum $C_w(T_n)$ is obtained from

$$C_w(T_n) = \int C(T_n, E_d) W(E_d) dE_d \tag{6}$$

where $C(T_n, E_d)$ is the distribution of the observed energy E_d deposited by the detected γ-ray and the observed TOF T_n related to the kinetic energy E_n of the incident neutron.

The not normalized experimental yield Y_{exp}, which is related to the fraction of neutrons that interact with the sample and creates a signal in the detection system, is

$$Y_{exp}(T_n) = \frac{C'_w(T_n) - B'_w(T_n)}{\varphi_n(T_n)} \tag{7}$$

where φ_n is the incident neutron flux and C_w' and B_w' are the observed dead-time corrected weighted count rates of the sample and background measurement, respectively. The incident neutron flux can be determined based on measurements of a standard cross-section [22]. At GELI-NA the neutron flux is simultaneously measured using either a ^{10}B or a ^{235}U ionization chamber placed in the neutron beam 1 m closer to the neutron source than the capture sample. The $^{10}B(n,\alpha)$ reaction is used for measurements below 150 keV and the $^{235}U(n,f)$ reaction for energies above 150 keV. At ORELA [19] and KURRI [21] the neutron flux is determined from measurements of the $^{10}B(n,\alpha\gamma)$ reaction using a ^{10}B sample in the capture detector set-up. The energy dependence of the neutron flux at n_TOF has been determined from measurements with a ^{235}U loaded parallel plate chamber [23] and is continuously monitored with a ^6Li deposit viewed by four silicon detectors [24].

The experimental yield Y_{exp} can be expressed as a function of the theoretical capture yield Y_c and scattering yield Y_n

$$Y_{exp}(T_n) = N \int R_T(T_n, E_n)(\varepsilon_{cw}(E_n) Y_c(E_n)$$
$$+ \varepsilon_{nw}(E_n) Y_n(E_n)) dE_n \tag{8}$$

where $R_T(T_n, E_n)$ is the neutron TOF resolution and expresses the probability that a neutron with an energy E_n will result in an event at time T_n. A detailed description of this resolution function for TOF-measurements carried out at GELINA can be found in Ref. [18]. The factor N is a normalization factor. The efficiency of the weighted response to detect a capture event or a scattered neutron is denoted by ε_{cw} and ε_{nw}, respectively. The latter ε_{nw} is the probability that a scattered neutron creates a detectable signal.

For non-fissionable samples and energies below the first inelastic scattering level, the capture and scattering yield can be expressed as a function of the total (σ_t), capture (σ_γ) and scattering (σ_n) cross-section by

$$Y_c(E_n) = (1 - e^{-n\sigma_t}) \frac{\sigma_\gamma}{\sigma_t} + Y_M \tag{9}$$

and

$$Y_n(E_n) = (1 - e^{-n\sigma_t}) \frac{\sigma_n}{\sigma_t} - Y_M \tag{10}$$

where n is the sample thickness in atoms/barn and Y_M accounts for the contribution of capture events after at least one neutron scattering in the sample. Full analytical expressions for both the capture and scattering yield, which are also valid for fissionable nuclei, are implemented in the REFIT code and can be found in Ref. [25]. The contribution due to the scattered neutrons, which will be discussed in more detail in Section 4, creates a time-dependent prompt background which cannot be distinguished from the real capture event and therefore contributes to the experimental yield.

Since in most cases the absolute neutron flux is not necessarily known and only the energy dependence can be accurately determined, the factor N in Eq. (8) is used to normalize the theoretical yields into experimental yields. This energy independent normalization factor N can be deduced from capture measurements at energies where the theoretical yield is well known. One can distinguish between normalization measurements based on a standard cross-section or based on a resonance for which the neutron width is much smaller than the radiation width ($\Gamma_n \ll \Gamma_\gamma$). The reference cross-section can be a thermal capture cross-section, or a standard cross-section in the higher region such as the $^{197}Au(n,\gamma)$ cross-section above 200 keV [22]. A normalization independent from any reference cross-section can be obtained from resonances with a neutron width that is much smaller than the radiation width. In the case when the macroscopic peak total cross-section is much less than unity ($n\sigma_t \ll 1$) the capture area is almost proportional to the neutron width and can be determined very accurately from independent transmission measurements. Examples of resonances strong enough to be observed in transmission measurements and their use in capture normalizations are the 1.15 keV resonance of ^{56}Fe [26] and the 2.25 keV resonance of ^{60}Ni [27].

For a saturated resonance the macroscopic total cross-section is much larger than unity ($n\sigma_t \ll 1$) and all incident neutrons with energies in the vicinity of the resonance energy interact with the sample [28]. The capture yield is in first approximation proportional to the ratio of the capture and total cross-section. If in addition, the neutron width is much smaller than the radiation width, the capture yield is close to unity. Suitable resonances to apply this so-called saturated resonance method are the 4.9 eV resonance of ^{197}Au and the 5.2 eV resonance of ^{109}Ag. The principle is illustrated in Fig. 2, where the capture yields for the 4.9 eV resonance of ^{197}Au for 4 different thicknesses are shown as
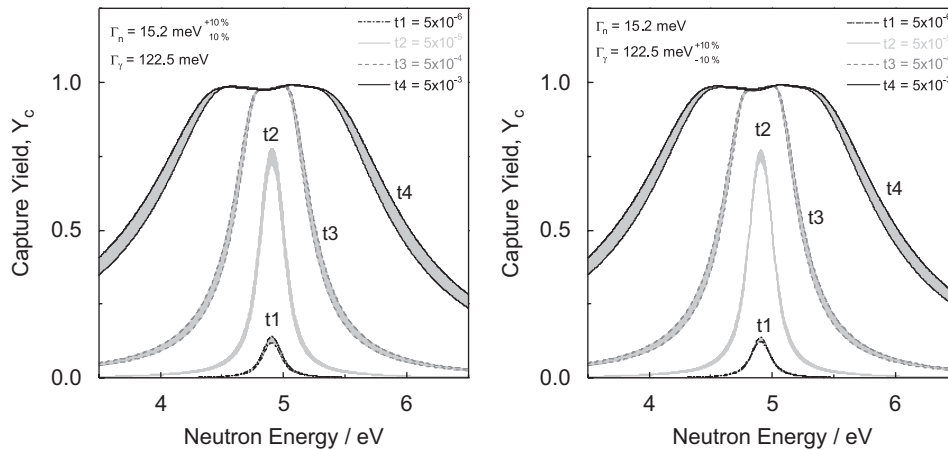
Fig. 2. The theoretical capture yield for the 4.9 eV resonance of Au. The yield is given for targets with different thickness (5×10^{-3}, 5×10^{-4}, 5×10^{-5} and 5×10^{-6} atoms/barn) and the impact of a total change of 20% in resonance parameters is shown by the grey region. The left panel shows the result for a change in neutron width and the right panel for a change in radiation width.

function of neutron energy. The capture yields have been calculated with the resonance shape analysis code REFIT [25] and include multiple scattering effects. The impact of a change in resonance parameters is shown by the grey region corresponding to a total change of 20% with respect to the JEFF 3.1 values in the neutron width (left panel) or the γ width (right panel). For the two smallest thicknesses the capture yields are not saturated, but for the two largest thicknesses the saturation is visible as a nearly flat top, at a level independent of the thickness. The structure in the top is due to multiple scattering. Fig. 2 indicates that a normalization obtained from a saturated resonance for which $\Gamma_n \ll \Gamma_\gamma$ is nearly independent of the resonance parameters and target thickness. Since the observed yield is not directly related to the capture area or peak cross-section but also depends on multiple scattering, it is hard to deduce resonance parameters obtained from only the fit to the capture yield of a saturated resonance.

3. Determination and validation of simulated weighting functions

To obtain reliable weighting functions an accurate response of the detection system $R_d(E_d, E_\gamma)$ is required for a set of γ-ray energies. This response depends on the γ-ray transport in the sample and the detector assembly. Consequently, the weighting function $W(E_d)$ must take into account the characteristics of both the detection system and the sample.

Corvi et al. [29,30] obtained for their set-up one single weighting function based on an experimentally determined detector response. The detector response was determined from measurements with radioactive sources and (p,γ) reactions on light nuclei. To account for the γ-ray transport in the sample the normalization was mostly based on measurements with a mixed target using the saturated resonance in Au or Ag or on a resonance with $\Gamma_n \ll \Gamma_\gamma$ measured with a thin target. Using the experimentally

determined weighting function, the capture area of the 1.15 keV resonance of ^{56}Fe for a thin sample was in agreement with the standard transmission value, after normalization at the saturated resonance at 5.2 eV of ^{109}Ag [29,30] and at 4.9 eV of ^{197}Au [31]. However, for very thick samples discrepancies up to 10% were observed [31]. More specifically, it was found that the derived value of the 1.15 keV capture area decreased with increasing sample thickness. Even using mixed targets accurate cross-section data could only be obtained if the γ-ray spectrum of the unknown did not vary strongly from the reference resonance. When the γ-ray spectrum of the reference sample differed greatly from the spectrum of the target under investigation, the use of a weighting function not accounting for the γ-ray transport in the sample resulted in systematic uncertainties as demonstrated by, e.g. Mutti et al. [32]. Using the experimental weighting function of Corvi et al. [30], the normalization factor based on the 1.15 keV resonance of ^{56}Fe in a mixed Pb–Fe sample was 7% smaller than the normalization factor based on the 5.2 eV ^{109}Ag resonance in a mixed Pb–Ag sample [32]. Therefore, the use of a single weighting function requires a special normalization procedure using mixed samples and a normalization resonance with a specific γ-ray spectrum. This is not always possible and often results in time-consuming measurements.

To avoid such a normalization procedure, Monte Carlo simulations can be used. Perey et al. [33] already successfully simulated response functions for C_6D_6 and C_6F_6 detectors using the γ-ray transport code EGS. Recently Wilson et al. [34] and the n_TOF collaboration [35] simulated the detector response for their C_6D_6 detection systems using the codes MCNP and GEANT. Abbondanno et al. [35] demonstrated that accurate weighting functions could be obtained from simulations provided that the geometry description reflects the experimental conditions. By applying a weighting function accounting for the γ-ray transport in the sample, Tain

et al. [36] simulated successfully the experiments of Corvi et al. [31], even the data for the thickest samples.

3.1. Determination of the detector response

In this work the MCNP code, version 4C3 [37], was used to determine the response of the capture detection systems to a series of mono-energetic γ-rays. The simulations were performed for a capture detection set-up installed at GELINA consisting of four C_6D_6-based liquid scintillator γ-ray detectors. The liquid for each NE230 scintillator was contained in an aluminium cylindrical cell 10 cm diameter and 7.5 cm height. Each cell was coupled to an EMI9823KQ photomultiplier through a boron free quartz window. Calculations were carried out for the detectors placed at 90° and 125° with respect to the direction of the incoming neutron beam. Great care was taken in describing the experimental conditions and in representing all the materials around the detector. Fig. 3 shows a two-dimensional view of the experimental set-up in the 125° geometry, as modelled in the MCNP geometry file. In the description of the detection system not only the active detection volume but also the aluminium canning, the boron free quartz window, the photomultiplier including the glass envelope, the electrical insulation and the flexible TEFLON tube were included. The latter serves as an expansion volume to compensate the thermal expansion of the C_6D_6. All these additional materials were especially important in the simulation of the neutron sensitivity (see Section 4). In the simulations, the response of each detector was treated separately but taking into account the whole environment.

Only the photon and electron transport in the sample and the detection system was calculated. The light production and its propagation in the scintillator were not taken into account. The final response was obtained by a convolution of the simulated response $R_e(E_e, E_\gamma)$ with a Gaussian function G, which represents the amplitude resolution of the detector

$$R_d(E_d, E_\gamma) = \int R_e(E_e, E_E) G(E_d - \mu(E_e)) dE_e \qquad (11)$$

with

$$G(E_d - \mu(E_e)) = \frac{1}{\sqrt{2\pi}\sigma_\mu} \exp\left(-\frac{(E_d - \mu(E_e))^2}{2\sigma_\mu^2}\right). \qquad (12)$$

In Eq. (11) the simulated response $R_e(E_e, E_\gamma)$ represents the transfer of a γ-ray energy E_γ in an electron energy E_e which is deposited in the detector. The conversion of the energy E_e into the observed energy is defined by the relationship $\mu(E_e)$ and a resolution broadening σ_μ, which are a function of E_e and $\mu(E_e)$, respectively. Ideally, $\mu(E_e)$ and σ_μ^2 are directly proportional to the energy E_e. To determine the functional relationships of the mean value and the variance together with the free parameters a similar procedure as discussed in Ref. [38] was applied. The experimental response for well-known mono-energetic γ-rays were compared with the simulated one obtained from the combination of Eqs. (11) and (12). The free parameters in the expressions for $\mu(E_e)$ and σ_μ^2 were determined by a least squares fitting procedure using experimental observed response functions. In order to determine the functional forms it is sufficient to fit the upper portion of the measured spectrum.

At γ-ray energies below 2.6 MeV standard radio-active sources can be used to determine the response of a detector. For higher energies the (p,γ) induced reactions on light nuclei [29,30,34,39] or capture γ-ray spectra from selected resonances of nuclei near closed shells can be used [33,40]. In this work spectra obtained for ^{137}Cs, ^{54}Mn, ^{65}Zn and ^{60}Co and selected resonances in ^{206}Pb(n,γ) were compared with results from simulations. The relative transition probabilities of the primary and secondary γ-rays for the resonances in ^{206}Pb(n,γ)

1 NE230 cell
2 Teflon
3 Quartz window
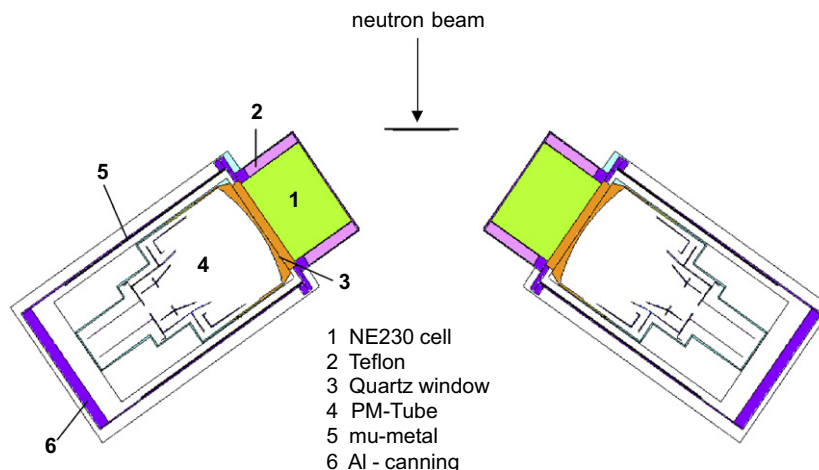4 PM-Tube
5 mu-metal
6 Al - canning

Fig. 3. Details of the geometrical description (horizontal cross-section) as implemented in the MCNP input file.

were taken from Refs. [41,42]. The simulated and experimental responses for γ-rays resulting from a ^{137}Cs source and for γ-rays of the 16 keV resonance in ^{206}Pb(n,γ) are compared in Figs. 4 and 5, respectively. For the radioactive sources the absolute detection efficiency was reproduced within 5%, close to the systematic uncertainty due to the determination of the position and the activity of the source. In Fig. 5 the relative contribution of the γ-ray cascades depopulating the capture state is shown. When the observed C_6D_6 spectra for the ^{206}Pb(n,γ) resonances were normalized to the simulated spectra in the region above 5 MeV, a good agreement below 1000 keV was observed without any adjustment of the relative intensities of the γ-rays in the cascades. Therefore, the good agreement in the whole energy region indicates that also the absolute efficiency in the high-energy region is well reproduced by the simulations. The resolution broadening, which corresponds to a FWHM of about 5% at 10 MeV, is comparable to resolution values of other liquid scintillators quoted in the literature [43].
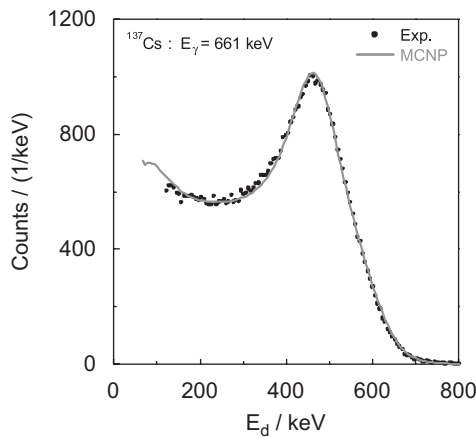

Fig. 4. Comparison of the experimental and simulated C_6D_6 response for the 661 keV γ-ray of a ^{137}Cs point source.
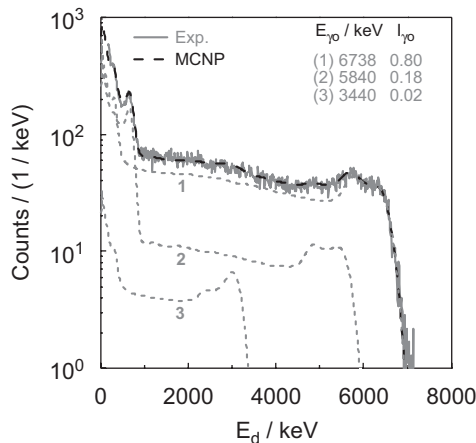

Fig. 5. Comparison of the experimental and simulated response for the γ-rays of the 16.4 keV resonance resulting from the ^{206}Pb(n,γ) reaction.

3.2. Determination of weighting functions

The good agreement between simulated and experimental response indicates that Monte Carlo calculations can be used to determine weighting functions, accounting for the complete measurement system including the sample material. The weighting function is obtained by expressing $W(E_d)$ as a smooth function of the observed deposited energy E_d and a set of free parameters. These parameters are obtained by a least squares fit to a number of γ-ray responses in the energy region of interest and minimizing the χ^2 defined by

$$\chi^2 = \sum_j \left(kE_{\gamma j} - \int_{E_L}^{\infty} R(E_d, E_{\gamma j}) W(E_d) dE_d \right)^2 \quad (13)$$

where E_L is a lower integration limit. The quality of the fitted weighting function can be addressed by calculating the quantity Q

$$Q = \frac{\int_{E_L}^{\infty} R(E_d, E_\gamma) W(E_d) dE_d}{kE_\gamma} \quad (14)$$

which has an expected value of 1, for each simulated response to an incident γ-ray with energy E_γ.

Due to experimental limitations it is impossible to record spectra at low values of the observed deposited energy due to the interference of noise and the use of a finite discriminator threshold E_D. To account for the missing part of the observed spectrum two approaches can be followed. In a first approach, the weighting function is calculated with $E_L = 0$ MeV in Eq. (13) and a correction is applied for the missing contribution of both the γ-rays for which the energy is below the experimental discriminator level E_D and the γ-rays that contribute only partly to the observed spectrum [44,45]. The former is obtained from tabulated transition probabilities. The latter can be obtained from Monte Carlo simulations. Another approach, which has been followed here, is to find the weighting function $W(E_d)$ for a finite discriminator level $E_L = E_D$ in Eq. (13) and correct for the missing contribution of γ-rays with an energy smaller than E_D. Applying the first approach, smaller deviations from unity of the values of Q as a function of γ-ray energy are obtained. However, the correction for the missing part of the observed spectrum in the first approach requires more information about the γ-ray emission spectrum and additional simulations.

In general, the best description of the weighting function can be obtained by applying a special unfolding technique to determine $W(E_d)$ in tabular form as carried out by Domingo et al. [44,45]. For point sources and thin samples the weighting function can be conveniently expressed as a 4th- [29,30] or 5th- [34] order polynomial. However, when the γ-ray transport in the sample material cannot be neglected, a simple polynomial is not sufficient. Under these conditions accurate weighting functions can be obtained by including negative powers in the polynomial

using the expression

$$\text{WF}(E_d) = \sum_{i=-3}^{4} a_i E_d^i. \tag{15}$$

In Fig. 6 the weighting functions for the detection system of Fig. 3 for two different configurations are compared. The corresponding detection efficiencies are shown in Fig. 1. The results in Figs. 1 and 6 are for the emission from a point source and for a homogeneous γ-ray emission from a Pb disc (1 mm thick and 60 mm diameter). The weighting functions were obtained with a discriminator level $E_L = 150 \text{ keV}$. The inset in Fig. 6 reveals that due to this discriminator level the weighting function significantly increases in the low energy region. In Fig. 7 the proportionality condition is verified by plotting the ratio
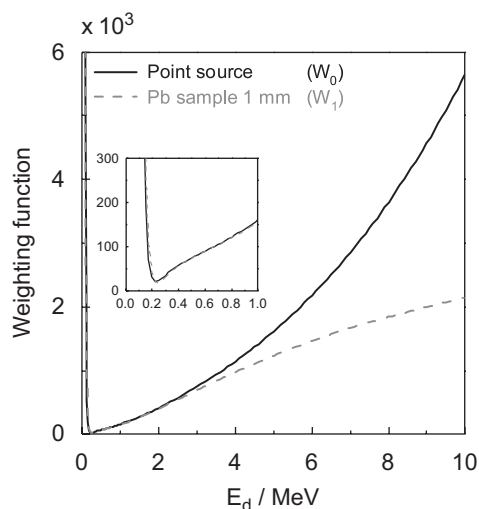

Fig. 6. The weighting functions for a γ-ray emission from a point source and a homogeneous emission from a Pb disc (1 mm thick and 60 mm diameter).
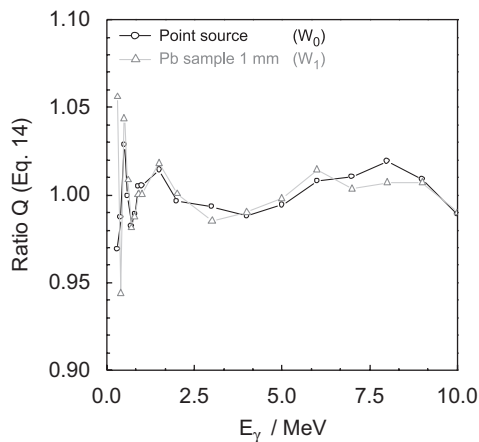

Fig. 7. Verification of the proportionality of the weighting functions shown in Fig. 6 by plotting the ratio Q defined in Eq. (14) as a function of the γ-ray energy.

Q defined in Eq. (14) as a function of the γ-ray energy. The maximum deviation from linearity is less than 5% and the relative standard deviation of this ratio is about 1.5%. The lower the threshold the better is the degree of linearity, as already noticed by Wilson et al. [34].

3.3. Validation of the weighting function

To validate the calculated weighting functions, capture cross-section measurements were performed at the neutron TOF-spectrometer GELINA of the Institute for Reference Materials and Measurements (IRMM) at Geel in Belgium [18]. The detection system consisted of four C_6D_6 detectors installed at a 60-m flight path station. The signals of the four detectors were treated by individual electronics. In case of the detection of coincident events, the signal of only one detector was taken at random. Therefore, only γ-rays from the same cascade interacting with the same detector could violate the condition of Eq. (1). Wilson et al. [34] studied in detail the impact of such events and observed a 0.6% bias effect for a 1.91% average detection efficiency. Measurements in two geometries were carried out with the detectors placed at 90° and 125° with respect to the direction of the incoming neutron beam. In both geometries the samples were placed perpendicular to the neutron beam. The experimental discrimination level of the capture detection system corresponded to $E_D = 150 \text{ keV}$. The shape of the neutron spectrum was measured with a triple Frisch-gridded ionization chamber placed at about 1 m before the sample. This chamber was loaded with three back-to-back layers of about 40 μg/cm^2 ^{10}B each. To deduce the experimental yield from the raw TOF-spectra the data processing package AGS was used [46]. More details about the data processing, such as dead time corrections and background subtraction, can be found in Refs. [46,47].

To study the impact of the γ-ray transport in the sample, the data were analyzed with three different weighting functions obtained from Monte Carlo simulations:

- W_0, which is valid for a point source in the centre of the neutron beam and only accounts for the γ-ray transport in the detection system and surrounding materials;
- W_1, which in addition to the detection system and surrounding materials also accounts for the γ-ray transport in the sample. The γ-rays are assumed to be homogeneously distributed throughout the sample;
- W_2, which accounts for the γ-ray transport in the detector and surroundings, but assumes a spatial distribution of the emitted γ-rays in the sample. This distribution accounts for the neutron flux attenuation within the sample.

In a first validation exercise the normalization factor N (see Eq. (8)) was determined with samples of different thicknesses and composition. The characteristics of the samples are specified in Tables 1 and 2. The REFIT code

Table 1
The normalization factors (relative to the adopted value) deduced from capture measurements in the 90° geometry obtained with the W_0, W_1 and W_2 weighting functions for samples with different characteristics (thickness, composition)

Sample	Ag (g/cm^2)	Pb (g/cm^2)	∅ (mm)	Weight (g)	Density (g/cm^3)	Thickness (mm)		Normalization factor $N/0.210$		
								W_0	W_1	W_2
Ag	0.088		60	2.483	10.49	0.08		1.041 (0.016)	0.974 (0.015)	1.005 (0.016)
Ag	0.191		60	5.413	10.49	0.18		1.017 (0.016)	0.963 (0.015)	0.993 (0.015)
^{nat}PbAg[a]	0.104	1.099	60	34.014	11.26	1.07		0.890 (0.014)	0.967 (0.015)	0.999 (0.015)
^{206}PbAg[b]	0.088	1.213	60	36.780	11.28	1.15		0.883 (0.014)	0.954 (0.015)	1.003 (0.016)
							Std. (%)	8.7	0.9	0.5

The normalization factors are deduced from the yield at the 5.2 eV saturated resonance of ^{109}Ag. The uncertainties (in parenthesis) are a combination of a 1.5% systematic uncertainty with the uncertainty resulting from counting statistics.
[a]Homogeneous mixture.
[b]Sandwich.

Table 2
The normalization factors (relative to the adopted value) deduced from capture measurements in the 125° geometry obtained with the W_0, W_1 and W_2 weighting functions for samples with different characteristics (thickness, composition)

Sample	Au (g/cm^2)	∅ (mm)	Weight (g)	Density (g/cm^3)	Thickness (mm)		Normalization factor $N/0.313$		
							W_0	W_1	W_2
Au	0.095	80	4.777	19.30	0.05		0.950 (0.014)	1.004 (0.015)	1.002 (0.015)
Au	0.217	80	10.920	19.30	0.11		0.926 (0.014)	1.004 (0.015)	1.001 (0.015)
Au	1.965	80	98.750	19.30	1.02		0.901 (0.014)	0.941 (0.014)	0.997 (0.014)
						Std. (%)	2.6	3.7	0.3

The normalization factors are deduced from the yield at the 4.9 eV saturated resonance of. The uncertainties (in parenthesis) are a combination of a 1.5% systematic uncertainty with the uncertainty resulting from counting statistics.

[25], which is based on the Reich–Moore approximation of the R-matrix formalism, was used to parameterize the data with only the normalization factor as an adjustable fit parameter. The code accounts for self-shielding, multiple scattering and Doppler effects and the resolution of the TOF-spectrometer. Details about the resolution of the GELINA facility can be found in Ref. [18]. The normalization factor was deduced from the saturated resonance of ^{109}Ag(n,γ) at 5.2 eV and of ^{197}Au(n,γ) at 4.9 eV from a fit in the energy region restricted to the resonance top. For the calculation of the theoretical yield in Eq. (8) the resonance parameters recommended in the JEFF 3.1 file were used. An example of such a fit for the 4.9 eV resonance in ^{197}Au(n,γ) is shown in Fig. 8. In Table 1 the normalization factors for measurements in the 90° geometry using the samples containing ^{nat}Ag are compared. The normalization factors for measurements in the 125° geometry based on the saturated resonance at 4.9 eV in ^{197}Au(n,γ) are given in Table 2. A spread of 1.5% in the normalization factors was deduced from a series of repetitive measurements from the same sample during a few months. This uncertainty is thought to be due to fluctuations in various components such as the changes in photomultiplier and/or amplifier gains of the capture detection system, the stability of the neutron monitoring system and variations in the sample position.
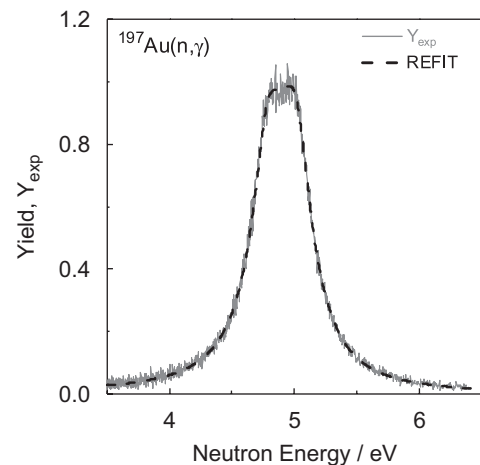

Fig. 8. The experimental yield for the 4.9 eV ^{197}Au is compared with the yield deduced from a resonance shape analysis using the REFIT code.

A comparison of the results in Tables 1 and 2 reveals that:

- The weighting function W_0, which does not include the effect of the γ-ray transport in the sample, results in a 15% lower normalization factor for the 5.2 eV resonance in the ^{206}Pb–Ag sample compared to that found in the thinnest Ag sample.

- For thick samples, with a high macroscopic neutron total cross-section, the data suffer from a systematic bias effect, when the coupling between the neutron and γ-ray transport is neglected. The normalization of the 1.1 mm thick Au gold sample is 6.6% different from the one obtained with the thin Au sample when this coupling is not taken into account.
- Using weighting functions, which also take into account the effect of both the γ-ray transport and the neutron flux attenuation in the sample, normalization factors agree to better than 1% and are independent of sample thickness.

For a final validation of the weighting functions the neutron width for the 1.15 keV resonance in ^{56}Fe(n,γ) was deduced from capture measurements in the 125° geometry with various samples. The characteristics of the samples are given in Table 3. The 1.15 keV neutron resonance of ^{56}Fe is an almost ideal case to test the accuracy of capture measurements [30]. This resonance is well isolated, and has a capture width which is about ten times larger than the neutron width. Therefore, the neutron width can be determined from both capture and transmission measurements. The normalization for the 60 and 80 mm diameter samples was based on the resonances at 5.2 eV of ^{109}Ag and 4.9 eV of ^{197}Au, respectively. Corvi et al. [30] noted that a measurement on ^{56}Fe–^{109}Ag provides a stringent test of the weighting function, even more severe than the most frequently used ^{56}Fe–^{197}Au normalization, because of the difference in the shape of the capture γ-ray spectra of the two nuclei. In the case of the 1.15 keV resonance [48], there

Fig. 9. The response of the capture detection system (distribution of the observed deposited energy) to the γ-rays of the 1.15 keV, 5.2 and 4.9 eV resonances in ^{56}Fe(n,γ), ^{109}Ag(n,γ) and ^{197}Au(n,γ), respectively.

are about 63 photons per 100 capture events with an energy above 6 MeV as compared to 5 and 19 γ-rays for the 5.2 eV ^{109}Ag and 4.9 eV ^{197}Au resonance, respectively [49]. Fig. 9 shows the response in the C_6D_6 detectors for the 1.15 keV ^{56}Fe, 5.2 eV ^{109}Ag and 4.9 eV ^{197}Au resonances. Since the γ-ray emission spectra for these resonances are different, there is a difference in the missed counts due to the finite energy threshold. Using the experimental γ-ray emission probabilities for the 1.15 keV ^{56}Fe, 5.2 eV ^{109}Ag and 4.9 eV ^{197}Au resonances [49], it was calculated that for a 150 keV threshold the observed response needed to be increased by 0.11%, 0.85% and 1.93%, respectively. According to Domingo [44] corrections due to the internal conversion process for γ-rays above 150 keV can almost be neglected.

The REFIT code was used to determine the neutron width for the 1.15 keV resonance of ^{56}Fe keeping the radiation width fixed at 574 meV. The results obtained from the analysis using the weighting functions W_0 and W_2 are listed in Table 3. Differences of up to 15% with respect to the standard transmission value $\Gamma_n = 61.7$ (0.9) meV of Perey et al. [26] occur when using the function W_0. Whereas the function W_2 gives an average value of $\Gamma_n = 62.3$ (1.0) meV and $\Gamma_n = 60.6$ (1.0) meV, for the data normalized via the Ag and Au resonance, respectively. These values are in very good agreement with the standard transmission value of $\Gamma_n = 61.7$ (0.9) meV and with the value $\Gamma_n = 61.8$ (1.9) meV deduced from capture measurements by Macklin [50]. In Ref. [50] the normalization to a saturated resonance of Au or Ag was avoided by a self-calibrating method using a thin and a thick laminated Fe sample and applying special corrections for the γ-ray attenuation in the sample.

4. Neutron sensitivity

The sensitivity of the detection system to neutrons plays an important role for all resonances with a neutron width much larger than the radiation width. This is the case for

Table 3
The neutron width of the 1.15 keV Fe resonance for capture in the 125° position using various samples containing ^{nat}Fe and applying the weighting function W_0 and W_2

Sample	g/cm^2		$\varnothing$ (mm)	Norm. sample	Γ_n (meV)	
	Fe	X			W_0	W_2
Fe1	0.105		60	Ag	53.3 (1.1)	62.6 (1.3)
Fe2	0.394		60	Ag	58.0 (1.0)	62.5 (1.1)
Fe3	0.905		60	Ag	57.9 (1.0)	60.2 (1.0)
^{206}PbFe[a]	0.394	1.213	60	Ag	62.4 (1.0)	63.1 (1.0)
PbFe[a]	0.422	1.103	60	Ag	63.1 (1.1)	62.6 (1.1)
PbFe[a]	0.422	2.725	60	Ag	59.2 (1.1)	62.6 (1.1)
Fe4	0.202		80	Au	55.4 (1.0)	61.2 (1.1)
Fe5	0.795		80	Au	60.6 (1.1)	60.3 (1.1)
Fe6	0.998		80	Au	61.2 (1.1)	61.2 (1.1)
AuFe	1.708	0.118	80	Au	62.9 (1.1)	61.3 (1.1)
Fe2O3	1.404	0.603	80	Au	55.8 (1.0)	59.1 (1.0)
				Mean	59.1	61.5
				Std	3.3	1.3
				Std (%)	5.6	2.1

The symbol 'X' denotes the element that, together with iron, is present in the sample. The uncertainties (in parenthesis) are a combination of a 1.5% systematic uncertainty with the uncertainty resulting from counting statistics. The sample used for normalization is also given.
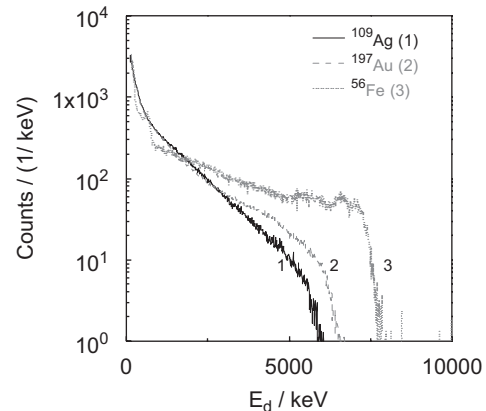
[a]Sandwich.

light nuclei and for heavier nuclei close to shell closures. To study such nuclei, detectors with the lowest neutron sensitivity have to be used and all materials surrounding the sample-detector assembly have to be reduced to a minimum. Plag et al. [17] discussed in detail the various components contributing to the neutron sensitivity and reported on a C_6D_6 detector with the lowest neutron sensitivity that has ever been achieved. The consequences of the neutron sensitivity on the resonance parameters of large s-wave resonances have been illustrated by Koehler et al. [16], Corvi [2] and Beer et al. [51]. After a substantial reduction of the neutron sensitivity of their detector system, Koehler et al. [16] determined a capture width for the 289 and 325 keV s-wave resonances in ^{88}Sr which was a factor five smaller than the previously published values. Corvi [2] compared the average radiation widths for s- and p-wave resonances of structural materials, i.e. $^{50,52,53}Cr$, $^{54,56}Fe$, and $^{58,60}Ni$, obtained at GELINA with C_6D_6 detectors with those obtained at ORELA using C_6F_6 detectors. The radiation widths for p-wave neutrons agreed within 20%. However, for large s-wave resonances the radiation widths obtained at ORELA were up to a factor 2 larger than those determined at GELINA. The influence of the neutron sensitivity in the determination of the resonance parameters for ^{208}Pb was demonstrated by Beer et al. [51]. They observed a linear increase of the ratio of the resonance capture area for $^{208}Pb(n,\gamma)$ reported by Macklin et al. [52] and values obtained at GELINA [51] with the ratio Γ_n/Γ_γ. These systematic differences reported by Corvi [2] and Beer et al. [51] are due to the difference in neutron sensitivity of the detection systems and/or the different methods to correct for it.

The neutron sensitivity of the GELINA detection system has been determined by Monte Carlo simulations with the code MCNP [37]. With today's Monte Carlo codes, the response to γ-rays can be calculated accurately. However, the simulation of the response to neutrons is less straightforward. For incident neutron energies below 1 MeV, the recoil energy deposit from neutron scattering is negligible and the neutron sensitivity is dominated by the γ-rays following capture of sample-scattered neutrons in the surrounding materials, and in a lesser extent from γ-rays following inelastic scattering. In most Monte Carlo codes reliable capture cross-section data required for neutron sensitivity calculations are used. The corresponding γ-ray spectra for most nuclei are only approximations. For the neutron-induced reactions in the simulations the photon production data from the evaluated data library JEFF 3.1 were used.

The results, which are shown in Fig. 10, were obtained for a $E_L = 150\,keV$ threshold. The ratio $\varepsilon_n/\varepsilon_\gamma$ of the probability that a neutron entering the assembly creates a signal, relative to the detection probability for a 4 MeV γ-ray is given as a function of the energy of the scattered neutron. In Fig. 11 the relative contributions of the different components are plotted as a function of neutron energy. The structures around the 5.9 and 35 keV Al
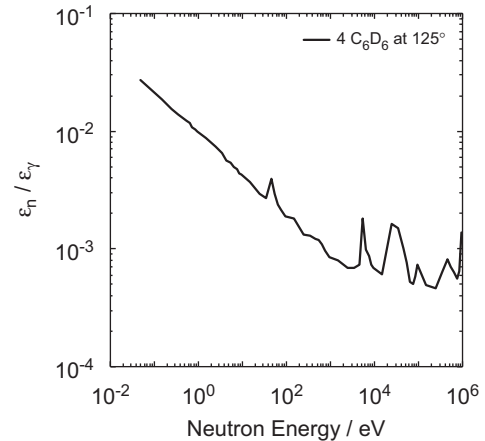

Fig. 10. The neutron sensitivity of the GELINA C_6D_6 capture detection system as a function of neutron energy. The ratio $\varepsilon_n/\varepsilon_\gamma$ of the probability that a neutron entering the system creates a detected signal relative to the detection efficiency for 4 MeV γ-ray is given as function of the neutron energy.
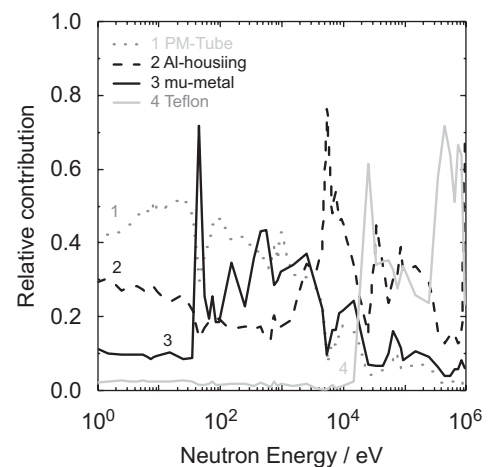

Fig. 11. The relative contribution of the neutron sensitivity of the different components of the capture detection system installed at GELINA.

resonances are smeared out due to the influence of multiple scattering effects. The contribution of fluorine present in the TEFLON tube surrounding the C_6D_6 volume, creates some structure around 100 keV. Due to the absence of fluorine in the scintillator material the neutron sensitivity for the C_6D_6 detector is significantly lower at the energies of the fluorine, resonances at 27 and 100 keV, as compared to the neutron sensitivity for C_6F_6 detectors [53]. Fig. 11 illustrates the strong impact of other materials such as the mu-metal which is 1.0 mm thick and the presence of the ^{10}B fraction in the glass tube of the photomultiplier. The influence of ^{10}B can be greatly reduced by setting an energy threshold above the 480 keV γ-ray from the $^{10}B(n,\alpha_1\gamma)$ reaction. However, this requires additional corrections as it will be discussed in Section 5. The simulations for the system consisting of four C_6D_6 detectors also indicated that the neutron sensitivity of each detector differs from the

one which would be obtained for a single detector without being surrounded by other detectors. An effect of the geometry and total number of detectors has also been noticed in Ref. [27]. Therefore, in the calculation of the neutron sensitivity of a detection system for neutron capture cross-section measurements the whole set-up, including sample changer and shielding materials, has to be taken into account.

The neutron sensitivity of the GELINA system has also been determined experimentally from capture measurements with a 10 mm thick graphite sample (80 mm diameter) and a 0.5 mm thick gold disc (80 mm diameter). A similar procedure was applied as the one described by Corvi [2] and Allen et al. [53]. For both the graphite and gold sample the same weighting function (i.e. homogeneous distribution in a 0.5 mm thick Au sample) was applied on the observed deposited energy. The weighted spectra were corrected for dead time and open beam background. The gold data were also corrected for the contribution of neutron scattering in gold. This contribution was estimated from the weighted response of the carbon sample, which was renormalized to the ratio of the macroscopic scattering cross-section of gold and carbon. Finally, the ratio between the weighted response due to a neutron entering the detector assembly (ε_{nw}) and the efficiency (ε_{cw}) to detect a capture event from the ^{197}Au(n,γ) reaction is obtained from the ratio between the net weighted count rates for the carbon and gold measurement, $C_{w,C}'$ and $C_{w,Au}'$, multiplied by the ratio of the ^{197}Au(n,γ) capture yield and the yield due to elastic scattering in ^{12}C

$$\frac{\varepsilon_{nw}}{\varepsilon_{cw}} = \frac{C_{w,C}'}{C_{w,Au}'} \frac{Y_{c,Au}}{Y_{n,C}}. \qquad (16)$$

The theoretical yields $Y_{c,Au}$ and $Y_{n,C}$ where calculated using the nuclear data in the JEFF 3.1 evaluated data file. Fig. 12 shows that the results obtained in this work are in
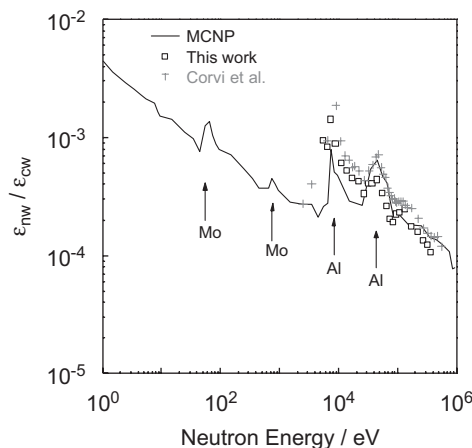
good agreement with the results obtained from simulations and with the data reported by Corvi [2], which were obtained for a similar detection system. The structures around neutron energies 45 and 500 eV result from Mo resonances due to the mu-metal shield of the photomultiplier. The structures around 6 and 35 keV are due to resonances in Al, which is present in the housing of the detectors. Due to the rather large contribution of the time dependent background $B_w'(T_n)$, it is difficult to deduce the net contribution of the neutron sensitivity and an averaging into relatively large time-bins was required. The discrepancies in Fig. 12 can be partly due to this averaging procedure. In addition, the simulated data have not been broadened to account for the resolution of the TOF-spectrometer.

Allen et al. [53] described a procedure, based on Monte Carlo simulations, to correct for the contribution due to neutron sensitivity and mentioned the importance to account for the multiple scattering contribution in the target. A similar, however analytical approach, is implemented in the REFIT code [25]. The contribution due to scattered neutrons is calculated by taking into account the kinematics of neutron scattering in the target and the additional flight path length due to the distance between the target and the detector. The code requires the probability ε_{nw} as a function of the energy of the scattered neutron. Since this efficiency is difficult to determine experimentally, the results of Monte Carlo simulations, which were validated by experiment, are used as an input. The impact of the neutron sensitivity was verified by a resonance shape analysis of a relatively strong s-wave resonance in ^{206}Pb(n,γ) using the REFIT code. For the neutron sensitivity applied in Eq. (8) the weighting function used to deduce the experimental yield Y_{exp} in Eq. (7) was applied. In Fig. 13 the experimental yield for the 160 keV resonance in ^{206}Pb(n,γ) together with the contribution due to the neutron sensitivity is shown. The overall contribution

Fig. 12. A comparison of experimental and simulated neutron sensitivity for the GELINA C_6D_6 capture detection system. The results are obtained by applying the weighting function for a 0.5 mm thick Au disc and are relative to the efficiency to detect a ^{197}Au(n,γ) capture event.
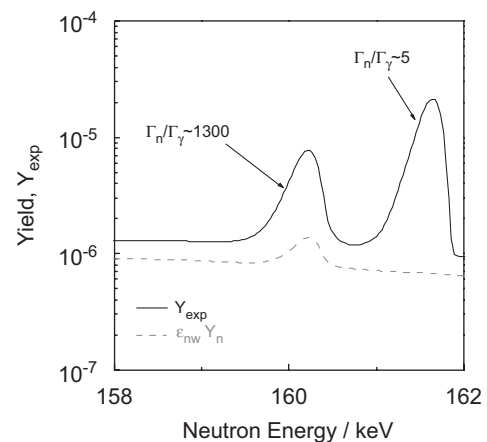

Fig. 13. The experimental yield obtained from capture measurements on a 1.08 mm thick ^{206}Pb sample is compared with the contribution due to neutron sensitivity of the detector assembly.

of the neutron sensitivity to the total resonance area of the 160 keV resonance is about 3%. From an analysis with REFIT a radiation width of $\Gamma_\gamma = 53.5$ meV is obtained. Not all analysis codes include a direct correction of the neutron sensitivity in the description of the experimental yield. Sometimes the radiation width is derived from the expression

$$\Gamma_{\gamma c} = \Gamma'_\gamma - \frac{\varepsilon_n}{\varepsilon_c}\Gamma_n \qquad (17)$$

where Γ'_γ is the radiation width resulting from the analysis without accounting for the neutron sensitivity. Applying such a procedure the radiation width for the 160 keV resonance $\Gamma_{\gamma c} = 48.3$ meV differs by 10% from the width deduced by a proper correction for the neutron sensitivity. The correction in Eq. (17) is only valid for very thin samples.

In the Unresolved Resonance Region (URR), the influence of the self-shielding and multiple scattering correction is mostly in the order of 1–2% and the resonance structure cannot be observed anymore. Therefore, the correction for the neutron sensitivity of the detection system can be directly applied on the experimental yield without introducing a significant bias effect. The contribution due to the scattered neutrons can be deduced from measurements with a sample with a similar neutron scattering probability however with a very low capture cross-section. To determine the average capture cross-section of ^{232}Th in the URR, Borella et al. [47] and Aerts et al. [54] corrected for the influence of neutron sensitivity by measurements of a ^{208}Pb sample with a similar thickness as the ^{232}Th sample.

5. Analysis of capture cross-section data

The results obtained in Section 3.3 demonstrate that for a given resonance the weighting function depends on the sample characteristics and the neutron flux distribution in the sample. Consequently, for a given sample the weighting function depends on the resonance strength and may differ from resonance to resonance. For weak resonances a homogeneous distribution of the γ-rays is valid, while for strong resonances one needs to account for the neutron flux attenuation. Hence, each resonance requires in principle its own weighting function. This is from a practical point of view not realistic. Therefore, for the analysis of capture data the following expression is proposed instead of Eq. (8):

$$Y_{exp}(T_n) = N \int R_T(T_n, E_n)(K_c(\sigma_t)\varepsilon_{cw}(E_n)Y_c(E_n)$$
$$+ \varepsilon_{nw}(E_n)Y_n(E_n))dE_n \qquad (18)$$

where the experimental yield Y_{exp} is deduced using the weighting function for a homogeneous distribution W_1 and K_c is a correction factor depending on the resonance strength. Since the yield due to the neutron sensitivity is not

affected by this phenomenon, one cannot correct the experimental yield and the correction factor needs to be applied on the calculated capture yield. For a correct application of Eq. (18), the detection efficiency ε_{nw} is obtained by applying W_1 for the sample under investigation.

The correction factor K_c can be deduced from the experimental data by analyzing the C_6D_6 response of resonances with a different strength and a similar γ-ray spectrum. The correction factor K_c is the ratio of the average weighting factor of the observed spectrum obtained with the weighting function W_1 and W_2. When the γ-ray emission spectrum is known the correction factor can also be obtained from Monte Carlo simulations by applying the weighting functions W_1 and W_2 on the spectrum emitted from a homogeneous distribution and a distribution depending on the total cross-section, respectively.

Fig. 14 shows the correction factor for a 0.1 and 1 mm thick Au sample as a function of the total cross-section multiplied by the target thickness, which is expressed in atoms/barn. The data are for a capture measurement system consisting of two C_6D_6 detectors installed at a 30-m flight path station of GELINA. The detectors, which were placed at 125° with respect to the direction of the incoming neutron beam, have a smaller effective detection volume compared to the set-up described in Fig. 3. The experimental data were deduced from the pulse height spectra of selected resonances. The simulated results obtained with MCNP were obtained for a ^{197}Au(n,γ) emission spectrum that was deduced with the program DICEBOX [55,56]. The γ strength functions and level densities were taken from the RIPL2 database [57] and the low energy level scheme from ENSDF. Fig. 14 shows the good agreement between the simulated and experimental data. For thin targets the correction factor can be
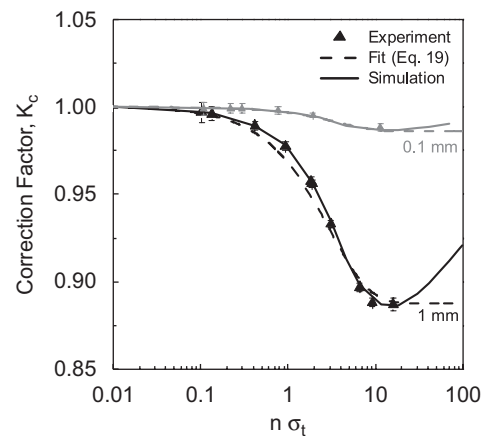

Fig. 14. The correction factor K_c as a function of the product of the target thickness and the total cross-section. The results obtained from an analysis of experimental spectra are compared with the results of simulations using the emission spectrum calculated with DICEBOX. The full line is the result of a fit using Eq. (19).

approximated by the expression

$$K_c(n\sigma_t) = \frac{1}{a + (1-a)e^{-bn\sigma_t}} \qquad (19)$$

where *a* and *b* are adjustable parameters depending on the target characteristics and on the γ-ray cascade. The results in Fig. 14 demonstrate that for thick targets such an analytical expression is only valid for small values of $n\sigma_t$. It has to be noted that the correction factor K_c not only depends on the target characteristics but also on the detector characteristics, geometry and surrounding materials. The correction factor for the 4.9 eV saturated resonance for measurements with the detection system used for the data in Fig. 14 is $K_c = 0.88$. This factor differs by about 7% from the factor $K_c = 0.94$ for measurements with the same target using the detection system of Fig. 3.

Other systematic effects such as:

(1) deviations from Eq. (4) due to limitations of the weighting function (see Fig. 7);
(2) the detection of coincident events;
(3) incorrect energy calibration and electronic drifts in the detection system;
(4) count losses due to the energy threshold;
(5) imperfect weighting due to the internal conversion process;
(6) imperfect weighting due to isomeric states

have already been studied and discussed extensively in Refs. [34,35]. In addition, Borella et al. [58] demonstrated that capture data (for e.g. ^{206}Pb(n,γ)) can suffer from a 20% bias effect when angular correlation effects are not taken into account.

All the above-mentioned effects depend on the specific character of the γ-ray cascade. Therefore, it is hard to evaluate an overall uncertainty level. The approach of Refs. [44,45], based on a Monte Carlo simulation of the γ-ray emission cascade, is very useful to estimate correction factors for individual cases. However, when the γ-ray emission cascade for the normalization reference is similar to the cascade for the sample under investigation, the influence of these effects is reduced. If in addition, an internal normalization is applied, i.e. the normalization is obtained from a resonance of the nucleus under investigation, all experimental conditions remain unchanged and the aforementioned 1.5% systematic uncertainty due to variations in sample position and detector and accelerator operating conditions is significantly reduced. Brusegan et al. [59] determined the ^{103}Rh(n,γ) thermal capture cross-section with an overall uncertainty of 1.0% from a combined analysis of capture and transmission data. The transmission data were used to determine the resonance parameters of the 1.26 eV resonance, with $\Gamma_n \ll \Gamma_\gamma$, which was used as an internal normalization resonance for the capture data. The ^{232}Th(n,γ) cross-section in the URR of Ref. [47] was deduced by normalizing the data to the yield of the quasi-saturated ^{232}Th resonances at 21.8 and 23.5 eV

with an uncertainty less than 2%. This uncertainty resulted mainly from the combined uncertainty due to the energy dependence of the neutron flux and the correction for self-shielding and multiple scattering. Borella et al. [47] demonstrated that in case of an internal normalization the impact of the weighting function on the final result was reduced to 0.5%. The normalized experimental yield deduced from the direct (not-weighted) count rates deviated by 0.5% from the one obtained from the weighted count rates. A similar discrepancy was observed when comparing the yield obtained with a weighting function that did not account for the γ-ray transport in the sample with the one deduced from a weighting function that accounted for this effect.

From the results in Table 3 and the work of Abbondanno et al. [35] one can conclude that experimental capture yields can be obtained with an accuracy of about 2% provided that weighting functions accounting for the γ-ray transport in the sample and for the influence of the resonance strength are applied. The results in Refs. [47,59] show that this uncertainty can still be reduced by applying an internal normalization based on a resonance for which $\Gamma_n \ll \Gamma_\gamma$. In case the resonance is not saturated and/or the experimental yield is sensitive to the resonance parameters, the normalization factor for the capture experiments can be deduced from a simultaneous analysis of capture and transmission data.

6. Conclusions

In this work, the use of C_6D_6 detectors for the determination of capture cross-section data in the resonance region is discussed, based on experimental data obtained at the TOF-facility GELINA. A procedure to apply the total energy detection principle in combination with the pulse height weighting technique is proposed. The procedure requires weighting functions accounting for both the γ-ray transport in the sample and the influence of the resonance strength and accounts for the influence of the neutron sensitivity of the detection system. The weighting functions and neutron sensitivity can be calculated using Monte Carlo simulations, provided that the geometry input file reflects the experimental conditions. Ideally the results obtained from simulations should be validated by experimental data, as was done in the present work. When the neutron sensitivity is important, additional correction factors need to be applied on the calculated capture yield and the correction for the neutron sensitivity needs to be incorporated in the resonance shape analysis. The correction for both the neutron sensitivity and the resonance strength are implemented in the latest version of the resonance shape analysis code REFIT. It has been demonstrated that by implementing the procedure proposed in this work capture cross-section data can be deduced with an uncertainty of 2%. This uncertainty can even be reduced by normalizing at an internal saturated resonance and/or by combining transmission and capture data.

Acknowledgements

We like to thank Wim Mondelaers and his staff for the skilful operation of GELINA. We are also grateful to J. Gonzalez for his technical support and to A. Moens for the preparation of the samples. We are also indebted to the reviewers of this paper for their constructive remarks.

References

[1] D.B. Gayther, R.B. Thom, Prompt gamma-ray detectors for the measurement of neutron capture cross-sections, Proceedings Meeting on Fast Neutron Capture, Argonne, April 1982, Report ANL-83-4, 1983, pp. 205–238.

[2] F. Corvi, The measurement of neutron capture cross sections via prompt gamma-ray detection, in: C. Coceva, et al. (Eds.), Proceedings Specialists Meeting on Measurement, Calculation and Evaluation of Photon Production Data, Bologna, November 9-11, 1994, Report NEA/NSC/DOC (95)1, pp. 229–246.

[3] A. Borella, A. Moens, P. Schillebeeckx, T. Van Bijlen, G.L. Molnár, T. Belgya, Zs. Révay, L. Szentmiklósi, J. Radioanal. Nucl. Chem. 265 (2005) 267.

[4] C. Coceva, Nuovo Cimento A 107 (1994) 85.

[5] T. Belgya, Phys. Rev. C 74 (2006) 024603.

[6] G.V. Muradyan, Yu.V. Adamchuk, Yu.G. Shchepkin, M.A. Voskanyan, Nucl. Sci. Eng. 90 (1985) 60.

[7] D.P. Barry, M.J. Trbovich, Y. Danon, R.C. Block, R.E. Slovacek, G. Leinweber, J.A. Burke, N.J. Drindak, Nucl. Sci. Eng. 153 (2006) 8.

[8] K. Kobayashi, S. Lee, S. Yamamoto, T. Kawano, Nucl. Sci. Eng. 146 (2004) 209.

[9] K. Wisshak, K. Guber, F. Käppeler, J. Krisch, H. Müller, G. Rupp, F. Voss, Nucl. Instr. and Meth. A 292 (1990) 595.

[10] K. Wisshak, F. Voss, F. Käppeler, G. Reffo, Phys. Rev. 42C (1990) 1731.

[11] P.F. Mastinu, the n_TOF collaboration, J. Phys.: Conf. Ser. 41 (2006) 352.

[12] J.L. Ullmann, U. Agvaanluvsan, A. Alpizar, E.M. Bond, T.A. Bredeweg, E.-I. Esch, C.M. Folden, U. Greife, R. Hatarik, R.C. Haight, D.C. Hoffman, L. Hunt, A. Kronenberg, J.M. O'Donnell, R. Reifarth, R.S. Rundberg, J.M. Schwantes, D.D. Strottman, D.J. Vieira, J.B. Wilhelmy, J.M. Wouters, The detector for advanced neutron capture experiments: a 4π BaF$_2$ detector for neutron capture measurements at LANSCE, Proceedings of the International Conference on Nuclear Data for Science and Technology, Santa Fe, NM, 2004, pp. 918–923.

[13] M. Heil, R. Reifarth, M.M. Fowler, R.C. Haight, F. Käppeler, R.S. Rundberg, E.H. Seabury, J.L. Ullmann, J.B. Wilhelmy, K. Wisshak, Nucl. Instr. and Meth. A 459 (2001) 229.

[14] M.C. Moxon, E.R. Rae, Nucl. Instr. and Meth. 24 (1963) 445.

[15] R.L. Macklin, J.H. Gibbons, Phys. Rev. 159 (1967) 1007.

[16] P.E. Koehler, R.R. Winters, K.H. Guber, T. Rauscher, J.A. Harvey, S. Raman, R.R. Spencer, J.C. Blackmon, D.C. Larson, D.W. Bardayan, T.A. Lewis, Phys. Rev. C 62 (2000) 055803-1.

[17] R. Plag, M. Heil, F. Käppeler, P. Pavlopoulos, R. Reifarth, K. Wisshak, Nucl. Instr. and Meth. A 496 (2003) 425.

[18] M. Flaska, A. Borella, D. Lathouwers, L.C. Mihailescu, W. Mondelaers, A.J.M. Plompen, H. van Dam, T.H.J.J. van der Hagen, Nucl. Instr. and Meth. A 531 (2004) 394.

[19] ⟨http://www.phy.ornl.gov/nuclear/orela/⟩.

[20] ⟨http://www.cern.ch/n_tof⟩.

[21] K. Kobayashi, Y. Fujita, N. Yamamuro, J. Nucl. Sci. Technol. 18 (1981) 823.

[22] F.-J. Hambsch, A.D. Carlson, H. Vonach, in: Proceedings of the International Conference on Nuclear Data for Science & Technology—ND2004, Santa Fe, NM, September 26–October 1, 2004, pp. 826–829.

[23] C. Borcea, the n_TOF collaboration, Nucl. Instr. and Meth. A 513 (2003) 524.

[24] S. Marrone, the n_TOF collaboration, Nucl. Instr. and Meth. A 517 (2004) 389.

[25] M.C. Moxon, J.B. Brisland, GEEL, REFIT, A least squares fitting program for resonance analysis of neutron transmission and capture data computer code, AEA-INTEC-0630, AEA Technology, October 1991.

[26] F.G. Perey, Status of the parameters of the 1.15-keV resonance of 56Fe, in: Proceedings of the International Conference on Nuclear Data for Basic and Applied Science, Santa Fe, NM, 1985, pp. 1523–1528.

[27] F. Corvi, G. Fioni, F. Gunsing, P. Mutti, L. Zanini, Nucl. Phys. A 697 (2002) 581.

[28] R.L. Macklin, J. Halperin, R.R. Winters, Nucl. Instr. and Meth. 164 (1979) 213.

[29] F. Corvi, A. Prevignano, H. Liskien, P.B. Smith, Nucl. Instr. and Meth. A 265 (1988) 475.

[30] F. Corvi, G. Fioni, F. Gasperini, P.B. Smith, Nucl. Sci. Eng. 107 (1991) 272.

[31] F. Corvi, G. Fioni, A. Mauri, K. Athanassopulos, Resonance neutron capture in structural materials, in: Proceedings of International Conference on Nuclear Data for Science and Technology, Jülich, Germany, 1991, pp. 44–47.

[32] P. Mutti, F. Corvi, K. Athanassopulos, H. Beer, P. Krupchitsky, s-process implications of 207Pb and 209Bi neutron capture cross sections, in: N. Prantzos, S. Harissoppulos (Eds.), Nuclei in the Cosmos V, Volos-Greece, Paris, 1998, pp. 204–207.

[33] F.G. Perey, J.O. Johnson, T.A. Gabriel, R.L. Macklin, R.R. Winters, J.H. Todd, N.H. Hill, Responses of C$_6$D$_6$ and C$_6$F$_6$ gamma-ray detectors and the capture in the 1.15-keV resonance of 56Fe, in: Proceedings of the International Conference on Nuclear Data for Science and Technology, Mito, Japan, 1988, pp. 379–382.

[34] J.N. Wilson, B. Haas, S. Boyer, D. Dassie, G. Barreau, M. Aiche, S. Czajkowski, C. Grosjean, A. Guiral, Nucl. Instr. and Meth. A 511 (2003) 388.

[35] U. Abbondanno, and the n-TOF collaboration, Nucl. Instr. and Meth. A 521 (2004) 454.

[36] J.L. Tain, the nTOF collaboration, J. Nucl. Sci. Technol. 2 (Suppl.) (2002) 689.

[37] J. Briesmeister, MCNP—A General Monte Carlo N-Particle Transport Code—Version 4C2, LA-13709-M, 2000.

[38] M. Weyrauch, A. Casnati, P. Schillebeeckx, M. Clapham, Nucl. Instr. and Meth. A 405 (1998) 442.

[39] D.B. Gayther, J.E. Jolly, R.B. Thom, Determination of the parameters of the 1.15-keV resonance in 56Fe by prompt gamma-ray detection, in: Proceedings of the International Conference on Nuclear Data for Science and Technology, Mito, Japan, 1988.

[40] A. Borella, Determination of the neutron resonance parameters for 206Pb and of the thermal neutron capture cross section for 206Pb and 209Bi, Ph.D. Thesis, Ghent University, 2005.

[41] M. Mizumoto, S. Raman, R.L. Macklin, G.G. Slaughter, J.A. Harvey, J.H. Hamilton, Phys. Rev. C 19 (1979) 335.

[42] M. Kadi, P.E. Garret, M. Yeh, S.W. Yates, T. Belgya, A.M. Oros-Peusquens, K. Heyde, Phys. Rev. C 61 (2000) 034307-1.

[43] G. Dietze, H. Klein, Nucl. Instr. and Meth. 193 (1982) 549.

[44] C. Domingo-Pardo, New radiative neutron capture measurement of 207Pb and 209Bi, Ph.D. Thesis, Universida de Valencia, 2004.

[45] C. Domingo-Pardo, the nTOF collaboration, Phys. Rev. C 74 (2006) 025807-1.

[46] C. Bastian, A. Borella, F. Gunsing, J. Heyse, S. Kopecky, G. Noguere, P. Siegler, P. Schillebeeckx, AGS, A Computer Code for Uncertainty Propagation in Time-Of-Flight Cross Section Data, Physor 2006, Vancouver, Canada, 2006.

[47] A. Borella, K. Volev, P. Schillebeeckx, F. Corvi, N. Koyumdjieva, N. Janeva, A. Lukyanov, Nucl. Sci. Eng. 152 (2006) 1.

[48] R.E. Chrien, M.R. Bhat, D.A. Wasson, Phys. Rev. C 1 (1970) 973.

[49] ⟨http://nds121.iaea.org/ensdf/reac_form.jsp⟩.

[50] R.L. Macklin, Nucl. Sci. Eng. 95 (1987) 200.

[51] F.H. Beer, F. Corvi, P. Mutti, Astrophys. J. 474 (1997) 843.

[52] R.L. Macklin, J. Halperin, R.R. Winters, Astrophys. J. 217 (1977) 222.

[53] B.J.Allen, A.R. deL. Musgrove, R.L. Macklin, Neutron sensitivity of capture gamma ray detectors, in: Proceedings of a Specialists' Meeting on Neutron Data of Structural Materials for Fast Reactors, Geel, Belgium, 1977, pp. 506–529.

[54] G. Aerts, the n_TOF collaboration, Phys. Rev. C 73 (2006) 054610-1.

[55] F. Bečvář, Nucl. Instr. and Meth. A 417 (1998) 434.

[56] F. Gunsing, F. Corvi, H. Postma, F. Bečvář, Nucl. Instr. and Meth. A 365 (1995) 410.

[57] ⟨http://www-nds.iaea.org/RIPL-2/⟩.

[58] A. Borella, A. Brusegan, M.C. Moxon, G. Aerts, F. Gunsing, P. Siegler, P. Schillebeeckx, High resolution neutron total and capture cross section measurements on ^{206}Pb, in: Proceedings of the International Conference on Nuclear Data for Science and Technology, Santa Fe, NM, 2004, pp. 1539–1542.

[59] A. Brusegan, E. Berthoumieux, A. Borella, F. Gunsing, M. Moxon, P. Siegler, P. Schillebeeckx, Neutron capture and transmission measurements on ^{103}Rh down to thermal energies, in: Proceedings of the International Conference on Nuclear Data for Science and Technology, Santa Fe, NM, 2004, pp. 953–956.